Atmospheric Plasma Deposited Dense Silica Coatings on Plastics

Linying Cui,[†,‡] Alpana N. Ranade,[§] Marvi A. Matos,[§] Liam S. Pingree,[§] Theo J. Frot,[||] Geraud Dubois,[‡,||,*] and Reinhold H. Dauskardt*[,‡]

[†]Department of Applied Physics, Stanford University, Stanford, CA 94305-4090, United States
[‡]Department of Materials Science and Engineering, Stanford University, Stanford, CA 94305-4034, United States
[§]Chemical Technology Division, Boeing Research and Technology, El Segundo, CA 90245, United States
[||]IBM Almaden Research Center, San Jose, CA 95120, United States

ABSTRACT: We explore the application of a high-temperature precursor delivery system for depositing high boiling point organosilicate precursors on plastics using atmospheric plasma. Dense silica coatings were deposited on stretched poly(methyl methacrylate), polycarbonate and silicon substrates from the high boiling temperature precursor, 1, 2-bis(triethoxysilyl)-ethane, and from two widely used low boiling temperature precursors, tetraethoxysilane and tetramethylcyclotetrasiloxane. The coating deposition rate, molecular network structure, density, Young's modulus and adhesion to plastics exhibited a strong dependence on the precursor delivery temperature and rate, and the functionality and number of silicon atoms in the precursor molecules. The Young's modulus of the coatings ranged from 6 to 34 GPa, depending strongly on the coating density. The adhesion of the coatings to plastics was affected by both the chemical structure of the precursor and the extent of exposure of the plastic substrate to the plasma during the initial stage of deposition. The optimum combinations of Young's modulus and adhesion were achieved with the high boiling point precursor which produced coatings with high Young's modulus and good adhesion compared to commercial polysiloxane hard coatings on plastics.

KEYWORDS: atmospheric plasma deposition, precursor chemical structure, silica molecular structure, elastic property, adhesion
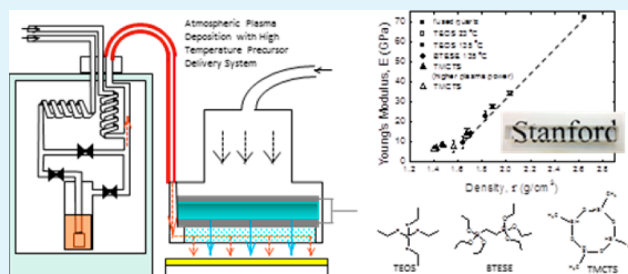
INTRODUCTION

Plastics, such as poly(methyl methacrylate) (PMMA) and polycarbonate (PC), are used in an expanding range of products from photovoltaic devices to airplane windows. These materials offer the advantages of relatively easy and cost-effective manufacturing and significant weight reductions when compared to other transparent materials such as glass. However, plastics usually have low hardness and a tendency to scratch, which can significantly reduce the performance of the final product and decrease the lifetime.[1] To overcome this challenge, transparent silica hard coatings are often deposited on plastic materials to improve their wear-resistance, hardness, transparency to light, and lifetime under UV and humid conditions. Besides the application of hard protective coatings on plastics, silica coatings can serve as a good permeation barrier to gas diffusion (when dense enough)[2] and a good wettability layer (when covered by silanol groups).[3] They can also be used in the fabrication of photovoltaic solar cells,[4,5] as corrosion resistant layers,[6] and in precision engineering (aeronautical and automotive).[7]

Silica coatings can be deposited with a variety of methods including sol–gel processes,[8] sputter deposition,[9] electron beam deposition,[10] and plasma enhanced chemical vapor deposition (PECVD).[11,12] More recently, it was reported that the deposition of silica was possible through the use of atmospheric plasma deposition.[13] Compared to plasma deposition under vacuum conditions, atmospheric plasma deposition is a more versatile technology and enables the deposition of coatings on large and/or complex geometry substrates. The versatility stems from the fact that vacuum equipment is not necessary, decreasing the initial capital investment and theoretically allowing for the deposition on substrates of any size and shape when integrated with other tools.[14] Plasma enhanced deposition techniques also have the advantage of minimal chemical waste throughout the process and are solvent-free compared, for example, to sol–gel techniques.[8] Finally, some plasma techniques including atmospheric plasmas work at low gas temperature, are suitable for treating plastics with low glass transition temperatures, and can even be used on biological samples.[14,15]

Several precursors have been reported for depositing silica coatings using atmospheric plasma deposition, including tetraethoxysilane (TEOS), tetramethylcyclotetrasiloxane (TMCTS), hexamethyldisilazane (HMDS), hexamethyldisiloxane (HMDSO), and tetramethyldisiloxane (TMDSO).[13] The application of a broader range of higher molecular weight precursors has been limited, however, by their higher boiling temperatures. For example, the carbon-bridged oxy-carbo-silane

precursors have been used to produce carbon bridged hybrid silica coatings by sol−gel processing, with the advantage of increased Young's modulus and adhesion/cohesion fracture energy.[16] However, their vapor pressures are less than 0.5 Torr at 100 °C, making standard atmospheric plasma deposition not feasible without a high-temperature precursor delivery system.

We explored the application of a high temperature precursor delivery system (Figure 1) for depositing high boiling point
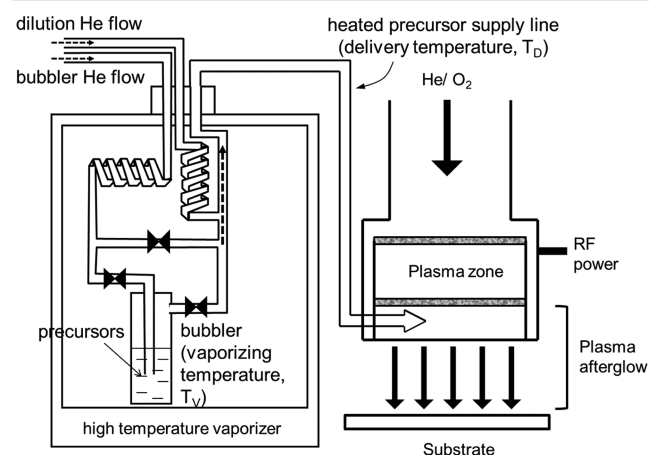

Figure 1. Schematic of the high temperature precursor delivery system and the atmospheric plasma deposition setup.

precursors on plastics using atmospheric plasma. We deposited coatings using a high boiling point carbon-bridged precursor, 1, 2-bis(triethoxysilyl)ethane (BTESE), and compared the coating's composition, molecular structure and mechanical properties to those deposited from two conventional precursors, TEOS and TMCTS. The effects of precursor delivery temperature and rate, functional groups, and the number of silicon atoms in the molecule, were studied and correlated to the coating properties, i.e. deposition rate, precursor incorporation efficiency, atomic content, molecular structure, density, Young's modulus, and adhesion energy to stretched PMMA substrate.

Interestingly, the deposition rate was shown to increase dramatically with elevated precursor delivery temperature and rate, more reactive functional groups, and larger number of silicon atoms in the precursor molecule. The precursor molecular structure and deposition condition also significantly influenced the coatings' mechanical properties. Namely, a linear relation between Young's modulus and coating density was observed, with the moduli ranging from 6 to 34 GPa. The coatings deposited from the TEOS precursor resulted in the highest density and Young's modulus values but exhibited low adhesion on PMMA in the range of 2.1−2.6 J/m². On the other hand, coatings deposited from BTESE had a good combination of Young's modulus and high adhesion energy up to 16.1 J/m² on the PMMA substrate. The TMCTS coatings had lower Young's modulus and adhesion energy of 3.0−5.1 J/m² than the BTESE coatings due to the different precursor molecular structure and resulting low coating density. The deposition rate, precursor chemical structure, coating network structure and density was found to be the important parameters to affect the adhesion of atmospheric plasma coatings on the PMMA substrate.

■ EXPERIMENTAL METHODS

Coating Deposition. An atmospheric pressure plasma deposition system (Surfx Technologies LLC, Los Angeles, CA) was employed to deposit the coatings. The area of the plasma showerhead was 5.1 cm². Research grade 99.995% purity quality helium and oxygen (Praxair Inc., Santa Clara, CA) were mixed and fed into the capacitive discharge plasma. The plasma was driven by 13.56 MHz radio frequency (RF) power. Reactive species were generated in the afterglow region of the plasma, including ground-state O atoms (atomic state ^{3}P), metastable molecular O_2 (atomic states $^1\Delta_g$ and $^1\sum_g+$), and ozone.[17] The densities of these reactive species were on the order of 10^{14} to 10^{15} cm^{-3}.[17,18] The plasma condition was kept constant in this study with 30 L/min helium, 0.5 L/min oxygen, and 60 W RF power, except for one TMCTS coating deposited with 30 L/min helium, 0.35 L/min oxygen, and 80 W RF power.

A carbon-bridged precursor, BTESE (Gelest, Inc. Morrisville, PA)[19] with a molecular weight of 354.59 g/mol and a vapor pressure of 0.3 Torr at 96 °C[19] was used to deposit coatings (Figure 2). Because the precursor vapor pressure was low

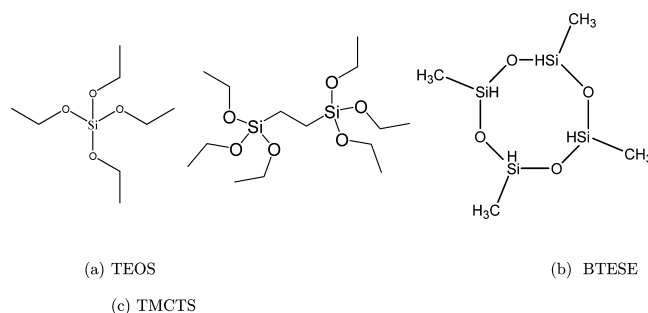

(a) TEOS   (b) BTESE

(c) TMCTS

Figure 2. Molecular structure of the precursors (a) tetraethoxysilane (TEOS), (b) 1,2-bis(triethoxysilyl)ethane (BTESE), and (c) tetramethylcyclotetrasiloxane (TMCTS).

below 100 °C, a high temperature vaporizer with a heated bubbler at temperature T_V, and a heated precursor delivery line at temperature T_D was constructed and integrated into the system (Figure 1). The resulting delivery system used helium gas to carry saturated vapor out of liquid BTESE which was held at T_V = 120 °C and had a vapor pressure around 1.6 Torr (calculated from the Clausius−Clapeyron relation). The saturated vapor balanced by helium was then heated to T_D = 135 °C and delivered to the immediate afterglow region of the plasma, where vaporized precursor molecules were activated through molecular collision reactions with radicals and other excited molecules.[14,20] Three different flow rates of the carrier helium gas were employed: 0.07, 0.10, and 0.20 L/min.

Silica coatings were also deposited from the precursors TEOS and TMCTS (Sigma-Aldrich, Saint Louis, MO) (Figure 2). For depositing TEOS, the precursor was first vaporized at T_V = 23 °C with vapor pressure around 1.5 Torr (molecular weight of 208.33 g/mol),[21] by passing 0.14 L/min helium gas through the TEOS liquid. Then the saturated TEOS vapor balanced by helium was delivered at either T_D = 23 or 135 °C to the immediate plasma afterglow region. For depositing TMCTS, the precursor was also vaporized at T_V = 23 °C, with vapor pressure around 7.1 Torr (calculated from the Clausius− Clapeyron relation).[22,23] Three different flow rates of the carrier helium gas were employed: 0.02, 0.10, and 0.39 L/min. The saturated TMCTS vapor balanced by helium was then

Table 1. Precursor Boiling Point, Vaporizing Temperature, Vapor Pressure, Carrier Gas Flow Rate, Precursor Molecule Vaporizing Rate, Si Atom Density in the Plasma Afterglow Region, and Precursor Delivery Temperature Used in This Study

precursor	boiling point	vaporizing temperature, T_V (°C)	vapor pressure (torr)	carrier gas flow rate (L/min)	precursor molecule vaporizing rate, R_V (μmol/min)	Si atom density in the plasma afterglow, N_{Si} ($\times 10^{14}$ atoms/cm^3)	precursor delivery temperature, T_D (°C)
TEOS	168 °C at 760 Torr	23	1.5	0.14	11.4	2.3	23
TEOS		23	1.5	0.14	11.4	2.3	135
BTESE	120 °C at 1.6 Torr	120	1.6	0.07	6.0	2.4	135
BTESE		120	1.6	0.10	8.7	3.5	135
BTESE		120	1.6	0.20	17.4	7.0	135
TMCTS	134 °C at 760 Torr	23	7.1	0.02	7.8	6.8	135
TMCTS		23	7.1	0.10	38	32.1	23
TMCTS		23	7.1	0.10	38	32.1	135
TMCTS		23	7.1	0.39	150	129.2	23
TMCTS		23	7.1	0.39	150	129.2	135

delivered at either T_D = 23 or 135 °C to the immediate plasma afterglow region.

Using the vapor pressure of the precursor and the helium carrier gas flow rate, the vaporizing rate of each precursor molecule was calculated. The precursor vapor gas balanced by helium was assumed to obey the ideal gas law $PV = nRT$, where P was the precursor partial pressure, V the total volume of the gas, n the moles of the precursor molecules, R the ideal gas constant, and T the temperature. Using the precursor vapor pressure for P and the carrier gas flow rate for V/(unit time), the mole of precursor molecules vaporized per unit time, R_V, could be calculated from $R_V = n/(\text{unit time}) = P \times (V/(\text{unit time}))/RT$ at the vaporizing temperature $T = T_V$. Note that although the BTESE precursor was vaporized at an elevated temperature of T_V = 120 °C, the value of carrier helium gas flow rate measured at room temperature before entering the precursor vaporizer could be used in the above equation. The reason was that the total pressure in the precursor delivery system with helium as the carrier gas was held constant at 1 atm and the vapor pressure of BTESE was much lower so that the resulting partial pressure of helium was almost constant at 1 atm thoughout the delivery system. Rearranging the ideal gas law to $V/T = nR/P$ for the helium gas, the right-hand side of the equation was constant before and after heating the gas, so we can equate the left side at two different temperatures

$$(V/T)_{T=23°C} = (V/T)_{T=120°C}$$

Thus, the BTESE molecule vaporizing rate is given by

$$R_V = \frac{n}{\text{unit time}} = P_{T=120°C}/R \cdot \left(\frac{V/T}{\text{unit time}}\right)_{T=120°C}$$
$$= P_{T=120°C}/R \cdot \left(\frac{V/T}{\text{unit time}}\right)_{T=23°C}$$

that is, the helium gas delivery rate measured at room temperature could be used directly to calculate the vaporizing rate of BTESE molecules held in a 120 °C bubbler.

Given the precursor molecule vaporizing rate, R_V, the Si atom density N_{Si} (atoms/cm^3) in the mixed flow of plasma and precursor delivery gases in the plasma afterglow region can be calculated by

$$N_{Si} = \frac{n_{Si}R_V N_A}{J_{plasma} + J_{precursor}}$$

where n_{Si} is the number of Si atoms in one precursor molecule, N_A the Avogadro's number, J_{plasma} the flow rate of the plasma gas, and $J_{precursor}$ the flow rate of the precursor gas.

The corresponding precursor vapor pressure, carrier gas flow rate, precursor molecule vaporizing rate, Si atom density in the plasma afterglow region, and precursor delivery temperature are summarized in Table 1. Note that the Si atom density in the plasma afterglow region were similar in two coating pairs: a TEOS coating deposited from 2.3×10^{14} Si atoms/cm^3 and a BTESE coating deposited from 2.4×10^{14} Si atoms/cm^3 in the plasma afterglow; and a BTESE coating deposited from 7.0×10^{14} Si atoms/cm^3 and a TMCTS coating deposited from 6.8×10^{14} Si atoms/cm^3 in the plasma afterglow.

Coatings were deposited on stretched PMMA and PC sheets (Makrolon Ltd., San Diego, CA), as well as on silicon (100) wafers. The substrate was wiped with ethanol before deposition to remove any surface contamination or dust and dried in air for 24 h. The substrate was placed 5 mm below the plasma source exposed to the plasma afterglow. Deposition of a uniform coating with controlled thickness was implemented through the use of an X−Y−Z robot that moved the plasma source over the substrate in a planar fashion forming a rectangular array. The speed of the plasma source was 50 mm/s. The spacing between neighboring lines was 0.3 mm.

Characterization Methods. The coating thicknesses on silicon, PC, and PMMA substrates were characterized by ellipsometry (Woollam M2000, J. A. Woollam Inc., Lincoln, NE). Incident light of 45° polarization was used for the measurement. The spectrum of the polarization of the reflected light versus wavelength was first taken for the coating on the silicon substrate. Software was used to fit the refractive index, absorbance, and/or thickness of the coating by regressive analysis based on the silicon substrate properties. A spectrum was then taken for the bare plastic substrate in the wavelength range of 250−1000 nm. Finally, a spectrum was taken for the coating on the plastic substrate. The difference in refractive index between the substrates and the coatings was enough to reflect sufficient light from the interface for the ellipsometry measurement. The measurement was also performed at the Brewster angle of the substrate to increase the detected signal. The coating thickness was fitted based on the measured refractive index and absorbance of the coating and substrate spectrum.

X-ray photoelectron spectroscopy (XPS) (Physical Electronics Inc., Chanhassen, MN) was used to characterize the atomic composition of the coating on the silicon substrates. An Al−K$_\alpha$ (1486 eV) X-ray source with a spot size of ∼1 mm was

used. Before the measurement, surface contamination was removed by Argon ion beam sputtering for 5 min, with a calibrated sputtering rate of 9 nm/min for the PECVD silica coatings. The scan range for the binding energy was 0−1000 eV. XPS was also used to characterize the atomic composition of the interfacial layer between the coating and the PMMA substrate. Argon ion beam was used to sputter off the material at a rate of 2 nm/min for the PECVD silica coating, with the setting of 1 kV, 0.5 μA, and 2 mm ×2 mm sputter spot. The angle between the detector and the sample surface was 45°.

The chemical bonds in the coating were characterized using IR spectroscopy. The spectrum was recorded as power dispersions in KBr using a Nexus 670 FT-IR (reflectance mode). Mid-IR in the wavelength range from 400 to 4000 cm^{-1} was probed at a resolution of 4 cm^{-1}. Coatings on silicon substrates were characterized either in transmission mode at the Brewster angle of the silicon substrate or in the total internal reflection mode by the Germanium attenuated total reflectory (ATR) accessory.

The density, ρ, of the coating on silicon substrate was measured by specular X-ray reflectivity (XRR) using a diffractometer (X'Pert Pro MRD, Panalytical, Westborough, MA) with ceramic X-ray tube (wavelength = 0.154 nm) and high resolution horizontal goniometer (reproducibility = ±0.0001 degree). The critical angle, θ_c, from the reflectivity data was obtained from the peak position of Iq^4 versus q plot, where I was the reflected X-ray intensity, $q = (4\pi/\lambda)\sin\theta$, λ is the wavelength, and θ is the grazing angle of the X-ray beam. The coating density ρ was inferred from the elecronic density ρ_e calculated using the equation

$$\rho_e = \left(\frac{\theta_c}{\lambda}\right)^2 \times \frac{\pi}{r_e} \times \frac{A}{Z} \times N_A$$

where r_e is the classical electron radius, A the atomic mass number, and Z the atomic number.

The Young's modulus was obtained using surface acoustic wave spectroscopy (SAWS). SAWS studies were performed with a laser-acoustic thin film analyzer (LaWave, Fraunhofer U.S.A., Boston, MA) in which acoustic waves were generated by a nitrogen pulse laser (wavelength 337 nm, pulse duration 0.5 ns). These were detected using a transducer employing a piezoelectric polymer film sensor. The measured surface wave velocity as a function of frequency was fitted with the theoretical dispersion curve to deduce Young's modulus (a value of 0.25 was assigned for Poisson's ratio).

The surface morphology of the atmospheric plasma treated PMMA surface was characterized by AFM (Park Systems XE-70 model scanning probe microscope, Park Systems Inc., Santa Clara, CA). Noncontact mode was used to prevent damage of the soft polymer surface, with a scan area of 1.267 μm × 1.267 μm and 1.7 μm Z range. The root-mean-square surface roughness was obtained using the software XEI equipped with the AFM.

The adhesion energy of the coating on PMMA was quantified using the asymmetric double cantilever beam (ADCB) test.[7,24−26] The specimens were prepared by bonding a blank (uncoated) substrate of 3 mm thickness onto a coated substrate of 6 mm thick. The in-plane dimensions of the specimen were 9 mm ×70 mm. The fracture tests were conducted on a micromechanical adhesion test system (DTS Delaminator Test System, DTS Company, Menlo Park, CA) in displacement control mode. The specimens were loaded at a displacement rate of 5 μm/sec in tension to produce controlled crack growth, followed by unloading. The load was measured simultaneously and the adhesion energy G_c (J/m^2), was calculated from the critical value of the strain energy release rate using[7,24−26]

$$G_c = \frac{6P_c^2}{E'B^2}\left[\left(\frac{a}{h_1} + 0.64\right)^2\frac{1}{h_1} + \left(\frac{a}{h_2} + 0.64\right)^2\frac{1}{h_2}\right]$$

where P_c was the load when the load−displacement curve deviated from linearity until initial crack extension, E' the plane strain Young's modulus of the substrate, B the substrate width, a the crack length, and h_1 and h_2 the substrate thicknesses. Application of the technique to thin hard coatings on softer substrates of similar type to the present study has been previously reported.[7]

■ RESULTS AND DISCUSSION

Deposition Rate and Incorporation Efficiency. The three different precursors, TEOS, BTESE, and TMCTS, were deposited to compare the effects of functional groups and the number of Si atoms in the precursor molecule on the deposition rate, r, (Figure 3a) and incorporation efficiency,
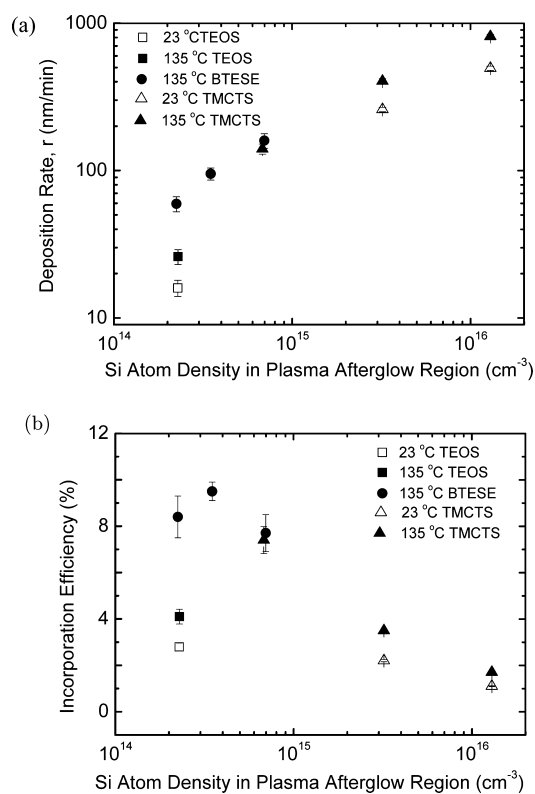

Figure 3. (a) Deposition rate and (b) incorporation efficiency of silica coatings on the PMMA substrate with different precursor supply conditions.

ξ_{Si} (Figure 3b). The incorporation efficiency ξ_{Si} was defined as the number of Si atoms incorporated in the coating divided by the total number of Si atoms in the precursor supply flow. It is straightforward to show that

$$\xi_{Si} = \frac{r\rho}{M_{SiC_xO_y}n_{Si}R_V}$$

6590

dx.doi.org/10.1021/am301723d | ACS Appl. Mater. Interfaces 2012, 4, 6587−6598

Table 2. Comparison of the Deposition Rate, Incorporation Efficiency, Density, Young's Modulus, and Adhesion Energy of Different Silica Coatings

coating type	precursor delivery temperature, T_D (°C)	Si atom density in the plasma afterglow, N_{Si} ($\times 10^{14}$ atoms/cm^3)	deposition rate, r (nm/min) (on PMMA)	precursor incorporation efficiency, ξ_{Si} (%) (on PMMA)	carbon content (excluding H) (atm %) (on PMMA and Si)	density, ρ (g/cm^3) (on Si)	Young's modulus, E (GPa) (on Si)	adhesion energy, G_c (J/m^2) (on PMMA)
TEOS atm plasma	23	2.3	16	2.8	0	2.035	34.2	2.6 ± 1.0
TEOS atm plasma	135	2.3	26	4.1	0	1.893	27.9	2.1 ± 1.0
BTESE atm plasma	135	2.4	59	8.4	0.8	1.707	14.2	4.4 ± 1.1
BTESE atm plasma	135	3.5	95	9.5	5	1.833	22.7	9.8 ± 1.9
BTESE atm plasma	135	7.0	159	7.7	8	1.645	9.5	16.1 ± 2.0
TMCTS atm plasma	135	6.8	140	7.4	3	1.565	7.7	3.6 ± 0.9
TMCTS atm plasma	23	32.1	259	2.4	9	1.472	8.50	3.0 ± 1.2
TMCTS atm plasma	135	32.1	404	3.7	7	1.480	8.16	3.6 ± 1.1
TMCTS atm plasma	23	129.2	494	1.1	13	1.423	6.85	4.3 ± 0.8
TMCTS atm plasma	135	129.2	810	1.8	11	1.406	6.13	5.1 ± 1.4
BTESE Sol gel (annealed at 400 °C)					29	1.5	21.8	
commercial polysiloxane coatings[7]							5	
fused quartz[52]					0	2.648	72	

where $M_{SiC_xO_y}$ is the molar mass of the SiC$_x$O$_y$ coating with the indices x and y determined by XPS elemental analysis. The effect of the TEOS and TMCTS precursor delivery temperature of 23 and 135 °C was also investigated. In addition, the effect of precursor delivery rate was studied with the BTESE and TMCTS precursors. The deposition parameters are summarized in Table 1. All the coatings were deposited in a plasma condition of 30 L/min helium, 0.5 L/min oxygen and 60 W RF power. The coatings up to 1 μm thick were deposited on the PMMA and PC substrates. The deposition rate was calculated from samples deposited on PMMA.

The TEOS coatings were deposited with the lowest Si atom density in the plasma afterglow region of 2.3×10^{14} atoms/cm^3. (Figure 3 and Table 2) The deposition rate was also the lowest: 16 ± 2 nm/min at precursor delivery temperature of $T_D = 23$ °C. It increased by 71% to 26 ± 3 nm/min at precursor delivery temperature of $T_D = 135$ °C. The corresponding incorporation efficiencies were 2.8 and 4.1%, respectively. Using the potentially more reactive precursor BTESE with similar Si atom density of 2.4×10^{14} atoms/cm^3 in the plasma afterglow region and at the delivery temperature $T_D = 135$ °C, the coating deposition rate was increased by more than twice to 59 ± 7 nm/min, together with a higher incorporation efficiency of 8.4%. The deposition rate of the BTESE coatings was further increased to 95 ± 9 and 159 ± 18 nm/min with higher Si atom density in the plasma afterglow of 3.5×10^{14} and 7.0×10^{14} atoms/cm^3. The corresponding incorporation efficiencies were 9.5 and 7.7%, respectively. For comparison, the deposition rate and incorporation efficiency of TMCTS precursor with Si atom denisty of 6.8×10^{14} atoms/cm^3 had a deposition rate of 140 ± 11 nm/min and incorporation efficiency of 7.4%, similar to its BTESE counterpart. With one and 2 orders of magnitude higher TMCTS delivery rate and Si atom density in the plasma

afterglow, the deposition rate increased further up to 810 ± 31 nm/min but the incorporation efficiency decreased down to 1.8%. In all the cases, the deposition rate and incorporation efficiency were significantly higher at the elevated precursor delivery temperature $T_D = 135$ °C than at $T_D = 23$ °C.

The results highlighted the significant effect of thermal activation of the precursor molecule on the deposition rate and the incorporation efficiency. The deposition rate increased by more than 50% in all cases when the precursor delivery temperature, T_D, increased from 23 to 135 °C. Because the plasma gas flow rate was much higher than the precursor vapor flow rate, the temperature of the mixed flow at the plasma source was almost solely determined by the temperature of the plasma gas flow while the elevated precursor delivery temperature only affected the initial stage of the reaction between the precursor molecule and the reactive species in the plasma afterglow. The marked enhancement of the deposition rate and the incorporation efficiency demonstrated the importance of the initial stage of the gas phase reaction in atmospheric plasma deposition. The activation energy of the precursor molecules was obtained from the Arrhenius equation $\ln(k) = \text{const} - E_a/RT$, where k was the reaction rate constant and proportional to the product of deposition rate and coating density, $r \times \rho$, (Table 2) for fixed reactant concentrations, and E_a the activation energy of the deposition reaction. The activation energy E_a can be extracted from the slope of $r \times \rho$ versus $1/T_D$ for a fixed precursor with fixed Si atom density in the afterglow. The calculated activation energy for the TEOS vapor with Si atom density of 2.3×10^{14} atoms/cm^3 in the afterglow was 0.89 kcal/mol. It increased marginally to 0.97 kcal/mol for the TMCTS vapor with Si atom density of 129.2×10^{14} atoms/cm^3, and to 1.04 kcal/mol for the TMCTS vapor with Si atom density of 32.1×10^{14} atoms/cm^3 in the afterglow.

Table 3. Bond Dissociation Energies of Some Si-Related Bonds[33−35]

bond	Me_3Si-H	Me_3Si-Et	$Me_3Si-OEt$	$Me_3SiO-Et$	$Me_3Si-OSiMe_3$	$Me_3Si-SiMe_3$	$H-CH_2OH$
dissociation energy (kcal mol^{-1})	94.6	92.3	122	98	136	79.3	96.1

The similar activation energies suggested that the reaction barriers for TEOS and TMCTS were similar. We note that the thermal energy increase by elevating the precursor delivery temperature from 23 to 135 °C, $\Delta E = 3R\Delta T$ ($\Delta T = 135-23$ °C) = 0.67 kcal/mol, which was large compared to the inherent deposition reaction activation energies. Note also that the activation energy for TEOS in atmospheric plasma deposition was lower than the reported activation energy of 6 kcal/mol for the first TEOS "chemisorption step" adsorbing onto a freshly deposited PECVD silica surface above 100 °C,[27,28] which was expected as the effect of the presence of reactive plasma species to reduce the deposition reaction barrier.

The increased deposition rate by thermal activation of the precursor has also been reported for aerosol-assisted CVD.[29] However, to our knowledge, there has not been any report of such an effect in the case of remote PECVD, although when depositing Si/H from silane (SiH_4) plasma, the silane gas temperature was shown to affect the coating molecular network order,[30] void formation, and refractive index.[31,32] The results in this study show the significant effect of preheating the precursor molecule before atmospheric plasma deposition to increase the deposition rate and incorporation efficiency, which is probably true for remote PECVD in general.

The precursor delivery rate was found to increase the deposition rate as shown by the results of the BTESE and TMCTS coatings with different precursor delivery rates. There was a general trend that with increasing Si atom density in the plasma afterglow region, higher deposition rate was achieved (Figure 3a). However, the incorporation efficiency dropped significantly when the Si atom density in the plasma afterglow region exceeded the reactive plasma species density, which was on the order of $10^{14}-10^{15}$ cm^{-3} [17,18] (Figure 3b). The higher precursor flow rate resulted in more porous coating, as evidenced by the lower coating density (Table 2).

The different functionalities in the precursor molecules also played an important role in the deposition. The dissociation energies of relevant bonds in Table 3[33−35] provide a general idea of the energy necessary to break bonds through collision with a neutral reactive oxygen species. For example, the dissociation energies of Me_3Si-Et (Me = methyl group, Et = ethyl group) and Me_3Si-H were 92.3 and 94.6 kcal/mol, lower than those of $Me_3SiO-Et$ (98 kcal/mol) and $Me_3Si-OEt$ (OEt = ethoxyl group) (122 kcal/mol). Having Si−C and Si−H bonds in the molecule, BTESE and TMCTS are more reactive than TEOS, which only has SiOEt functional groups.

Comparing the 135 °C TEOS and BTESE coatings with similar Si atom density of 2.3−2.4 × 10^{14} atoms/cm^3 in the plasma afterglow, the BTESE coating had more than twice higher deposition rate and incorporation efficiency than TEOS. That was due to the more reactive carbon bridge functionality in the BTESE molecule than the ethoxyl groups in TEOS. In addition, the carbon bridge between the two Si atoms in the BTESE molecule makes the activation of the Si atoms by collision with reactive oxygen species more productive. When an oxygen reactive species collides with the carbon bridge in the BTESE molecule, the two Si atoms at the two ends of the bridge can be simultaneous actived, if the collision is successful. In contrast, one effective collision for the TEOS molecule can only activate a single Si atom. So larger amount of Si atoms can be activated in the case of BTESE than in TEOS.

The four-membered siloxane ring in the TMCTS molecule also contributed to higher deposition rate and incorporation efficiency. During depositing TMCTS, the four-membered siloxane rings reacted with each other through breaking the highly reactive Si−H bond and form multiringed silicate structures. Since both gas phase and surface reactions are considered important in atmospheric plasma deposition and adsorption is thought to be the rate-limiting step for precursors, such as TEOS, with low sticking probability,[36] the large multisiloxane ringed clusters with low diffusion coefficients on the coating surface[37,38] should have high surface adsorption rate and correspondingly high deposition rate and incorporation efficiency. Comparing the BTESE and TMCTS coatings pair deposited with similar Si atom density of 6.8−7.0 × 10^{14} atoms/cm^3 in the plasma afterglow region, the deposition rate and incorporation efficiency were similar. So TMCTS is also more readily deposited by atmospheric plasma than TEOS.

Although further studies are needed to fully ellucidate these reaction pathways, the deposition rates in the order of BTESE ≈ TMCTS > TEOS were confirmed. We note finally that the deposition rates observed were comparable to literature reported values for atmospheric plasma deposition of glass coatings on plastics.[13] By choosing different precursors, a wide range of deposition rate could be achieved using identical plasma condition and similar precursor delivery parameters.

Atomic Content and Molecular Structure. Coating molecular structure, density, and Young's modulus were characterized on silica coatings deposited on silicon substrates under identical conditions as previously described. This allowed us to use characterization techniques such as IR, XRR and SAWS that would be more difficult to use on the polymer substrates.

The atomic content of the coatings on PMMA and Si substrates was measured by XPS and related to the precursor structure and deposition conditions. Hydrogen was not included in the atomic composition calculation due to limitations of the technique. The molecular structure of the coatings was characterized by IR. Both the Si−O−Si network and the chemical state of the carbon remnant were found to vary in the coatings deposited from different precursors.

All the coatings deposited from TEOS, BTESE, and TMCTS had atomic compositions similar to that of silica. The TEOS coating deposited with low Si atom density of 2.3 × 10^{14} atoms/cm^3 in the plasma afterglow was almost pure silica, with 31 atm% of Si, 69 atm% of O, and C below the detection limit of XPS. No composition difference was observed for the coatings deposited from 23 and 135 °C TEOS vapors. The BTESE coatings deposited with Si atom densities of 2.4, 3.5, and 7.0 × 10^{14} atoms/cm^3 in the plasma afterglow had crabon content of 2, 5, and 8 atm%. The carbon remnant probably came from some preserved carbon bridges and incompletely oxidized ethyl and ethoxyl groups, given the higher deposition rate and resulting lower chance for complete oxidation, as well as the limited reactive oxygen species from plasma. Similarly, the TMCTS coatings had carbon residues. Because the reaction between the Si−H groups and reactive oxygen species played

the main role to form the silicate network, many of the Si−Me group were not completely oxidized. The carbon content in the TMCTS coatings ranged from 3 to 11 atm% (Table 2). The coatings deposited at a higher precursor delivery temperature $T_D = 135$ °C had lower carbon content because of a thermally enhanced oxidation reaction. Another trend is increasing the BTESE and TMCTS precursor delivery rate increased the carbon content because of the limited amount of reactive oxygen species available to maintain the same oxidation level.

The chemical forms of the carbon species as well as other chemical bonds present in the coatings were characterized by IR (Figure 4a). In the spectra for the TEOS, BTESE, and TMCTS coatings, strong bands associated with the asymmetric stretching, bending and rocking modes of the Si−O−Si bond were observed at ∼1075 and 800 cm^{−1}.[12,13,36] The shape difference of the bands at ∼1075 cm^{−1} resulted from different molecular network structures of Si−O−Si as discussed below. The band at ∼930 cm^{−1} was attributed to Si−OH stretching mode,[39] commonly observed for PECVD coatings grown at reduced temperature.[39−41] This result was consistent with the broad band observed at ∼3400 cm^{−1} for hydrogen-bonded O−H groups.[13] The IR spectra of the TEOS coatings confirmed the XPS results that the TEOS coatings were almost pure silica coatings, with minute carbon residues. For the 23 °C TEOS coating, no carbon related peaks were observable, while for the 135 °C TEOS coating, very small peaks between 1400 and 1800 cm^{−1} were observed, although the carbon content was below the detection limit of 1 atm% by XPS. Also note that in the TEOS coating spectra, a shoulder at 3650 cm^{−1} was observed due to O−H stretching vibration of isolated hydroxyl groups.[13] This suggested that the Si−O−Si network of the TEOS coatings were denser than those of the BTESE and TMCTS coatings, with less terminal groups. The band at ∼2140 cm^{−1} in the spectra of the TMCTS coatings was due to Si−H stretching,[39] indicating the abundance of Si−H groups compared to reactive oxygen species and the resulting Si−H remnants in the TMCTS coatings.

In addition, there were carbon related peaks and bands.[12,36] The bands at 780, 1275, and 1410 cm^{−1} in the TMCTS coating spectra were due to Si−CH$_3$ rocking,[42,43] deformation[39,43] and asymmetric bending,[39,43] respectively, indicating that some of the Si−CH$_3$ species in the TMCTS monomer were not reacted and were incorporated in the coating. Comparing the spectrum of the TMCTS monomer[44] to those of the TMCTS coatings, we noticed that there was more reduction of the Si−H band at ∼2140 cm^{−1} than the Si−CH$_3$ band at ∼1275 cm^{−1} in the TMCTS coating spectra, suggesting that the Si−H group was more reactive than the Si−CH$_3$ group in the oxygen atmospheric plasma. Heating the TMCTS vapor did not result in a large effect on the molecular structure of the coatings probably because of the overall high percentage of carbon remnants in the coatings.

In the spectrum of the BTESE coating deposited with Si atom density of 7.0×10^{14} atoms/cm^3 in the plasma afterglow region, there were characteristic absorption bands at 2870−2920 cm^{−1} for sp^3 C−H stretching vibrations, together with CH$_2$ vibrations at ∼1270 and ∼1410 cm^{−1}, which could be regarded as evidence for the presence of Si−CH$_2$−CH$_2$−Si structures in the silica network.[45] By comparison, in the spectrum of the BTESE coating deposited with Si atom density of 3.5×10^{14} cm$^{−3}$ in the plasma afterglow region, the absence of the bands at ∼750 and 1275 cm^{−1} for the Si−CH$_2$/Si−CH$_3$ bending mode[42,44] suggested that almost all the carbon bridges
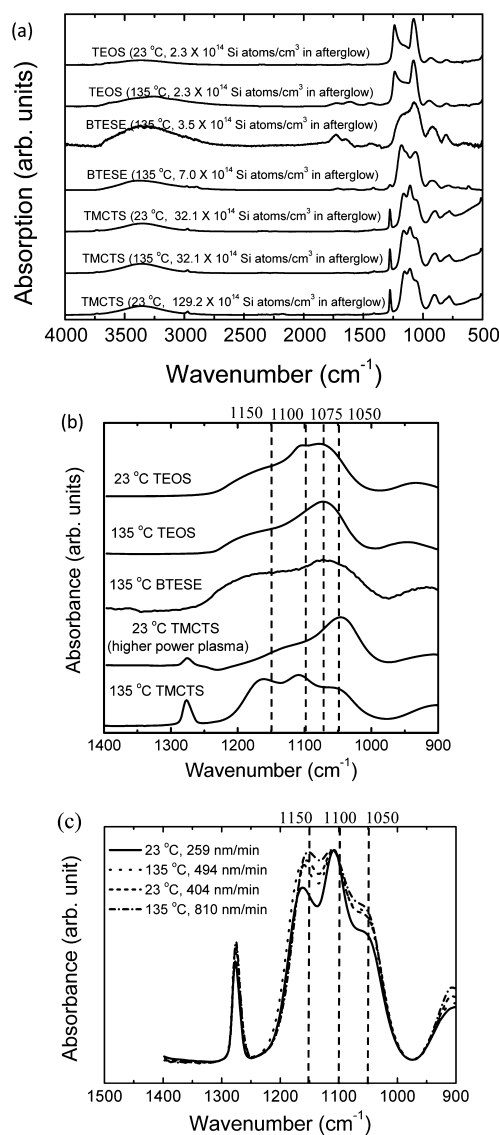

Figure 4. FTIR spectra of (a) the 23 and 135 °C TEOS coatings, 135 °C BTESE coatings (Si atom density in the plasma afterglow region = 3.5 and 7.0×10^{14} atoms/cm^3), 23 and 135 °C TMCTS coatings (Si atom density in the plasma afterglow region = 32.1×10^{14} atoms/cm^3), and 23 °C TMCTS coatings (Si atom density in the plasma afterglow region = 129.2×10^{14} atoms/cm^3); (b) the Si−O−Si band for the 23 and 135 °C TEOS coatings (ATR mode), 135 °C BTESE coating (Si atom density in the plasma afterglow region = 3.5×10^{14} atoms/cm^3), 23 °C TMCTS coating with higher plasma power, and 135 °C TMCTS coatings (Si atom density in the plasma afterglow region= 32.1×10^{14} atoms/cm^3); and (c) the Si−O−Si band for the four TMCTS coatings with different deposition rates.

were oxidized during deposition, while the bands at ∼1470 cm^{−1} were due to residual Si−O−C species.[46] The band at ∼1725 cm^{−1} was attributed to C=O stretching mode,[47] consistent with the above observation that almost all the carbon residues in the BTESE coating were in the oxidized state, some even in the highly oxidized C=O state. The peak at ∼2950 cm^{−1} was due to C−H stretching.[36,48]

The XPS and IR results suggested that a Si−O−Si network was formed in the TEOS, BTESE and TMCTS coatings. The TEOS coating had almost no carbon remnants. The BTESE coating had a few carbon remnants, in the form of ethyl carbon bridges and oxidized carbon species. The TMCTS coatings

with high deposition rates had the most carbon preserved, some in its pristine state. The difference in carbon content resulted from the different chemical structures and functionalities of the precursor molecules. For the TEOS precursor, starting from the smallest building block—a single Si atom in every molecule, the four SiOEt groups are well exposed to reactive oxygen species and they have to be well reacted with other TEOS molecules and oxygen species to form a silicate cluster with large enough size and low enough diffusion coefficient to promote the adsorption on the surface.[36,37,49] In such a case, the oxidation reaction was quite complete, leading to a highly dense, well-formed Si−O−Si network with almost no carbon residues. The TMCTS four-membered siloxane ring structure serves as a preformed nucleus for cluster formation. Coupled with the high reactivity of the Si−H groups, multiringed silicate clusters with carbon terminal groups at some sites can easily form and adsorb on the surface, resulting in hybrid silica coatings containing the siloxane rings and Si−Me groups, with high deposition rates. For the BTESE molecule, with low precursor molecule density in the plasma afterglow region, the Si−C−C−Si bridges were almost all oxidized by the abundant reactive oxygen species; while with higher BTESE molecule density in the plasma afterglow, the reactive oxygen species became limited and carbon bridged precursor species could adsorb onto the coating surface before getting oxidized. Note that depositing films containing carbon bridges between silicon atoms was previously demonstrated in vacuum by PECVD.[48]

Coating Density and Young's Modulus. The density and Young's modulus of the coatings on Si substrate showed a negative correlation with the deposition rate (Figure 5a, Table 2). Similar trends were observed for PECVD hard carbon
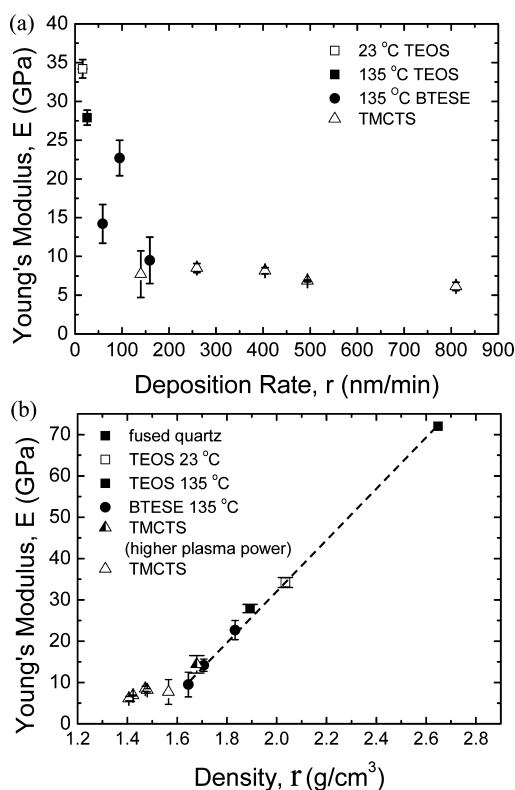

Figure 5. Relation between (a) Young's modulus and deposition rate and (b) Young's modulus and density of the atmospheric plasma coatings.

coatings[50] and tungsten nanostructures grown by focused ion beam-induced CVD.[51] With the lowest deposition rate, the TEOS coating deposited from the 23 °C precursor vapor had a density of 2.04 g/cm^3 and a Young's modulus of 34.2 ± 1.2 GPa. Interestingly, the TEOS coating deposited from the 135 °C precursor vapor had a lower density of 1.893 g/cm^3 and lower Young's modulus of 27.8 ± 1.0 GPa. Corresponding to the higher deposition rate, the densities of the atmospheric plasma BTESE coatings was lower in the range of 1.645−1.833 g/cm^3 and the Young's moduli were 9.5−22.7 GPa. For comparison, the sol−gel BTESE coating required a postannealing at 400 °C to achieve a density of 1.5 g/cm^3 and Young's modulus of 21.8 ± 0.5 GPa.[16] The density and Young's modulus of the TMCTS coatings were the lowest given their highest deposition rates. The coating densities were in the range of 1.406−1.565 g/cm^3 and the Young's moduli were 6.13−8.50 GPa. For reference, commercial polysiloxane coatings deposited by sol−gel processes typically exhibit a Young's modulus around 5 GPa,[7] and fused quartz has a Young's modulus of 72 GPa.[52] The high Young's moduli obtainable in the present coatings demonstrate the capability to deposit such dense coatings by atmospheric plasma at temperatures below 100 °C.

It has been shown that the mechanical properties of silicate and organosilicate can be correlated to their network connectivity.[53] For instance, the type of Si−O−Si bond structures directly influences the network connectivity per unit volume. Such structures can be elucidated by looking at the FTIR spectra in the 1000−1200 cm^{-1} region (Figure 4b). In our coatings, the broad band from 1000−1200 cm^{-1} was due to the Si−O−Si asymmetric stretching mode, typical for a siloxane network. This band consisted of several overlapping peaks corresponding to Si−O−Si bonds in different configurations. The peak at 1075 cm^{-1} was assigned to the stretching of Si−O−Si bonds in a fully relaxed SiO$_2$-network structure with bond angle ~144°.[44,54] The peak at 1100 cm^{-1} was attributed to larger angle Si−O−Si bonds in a network structure.[44,54] The peak at 1150 cm^{-1} was indicative of highly symmetric siloxane ring structure, such as T$_8$ cages (Figure 6),[55] while the peak at

T$_8$ cage (R$_8$Si$_8$O$_{12}$)   Open T$_7$ cage (R$_7$Si$_7$O$_{12}$H$_3$)
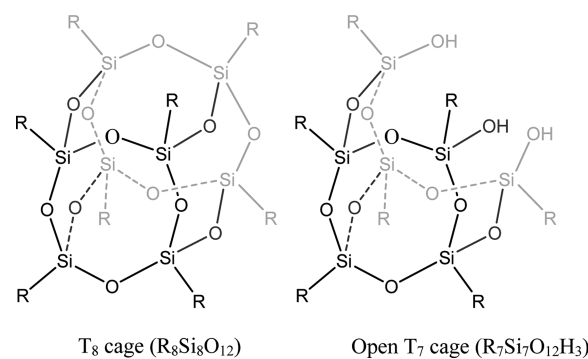
Figure 6. Structure of highly symmetric T$_8$ cage and lower symmetric T$_7$ cage.

1050 cm^{-1} was due to less symmetric and more random network structure, such as T$_7$ open cages (Figure 6), although still having local symmetry around the Si−O−Si unit.[55] The cage and siloxane ring structures resulted in lower network connectivity,[55,56] and consequently reduced Young's modulus.[53]

As shown in Figure 4b, the TEOS coating deposited from 135 °C precursor vapor which had lower Young's modulus had only one peak at 1075 cm^{-1}, suggesting a well-formed Si–O–Si network. Surprisingly, the coating deposited from 23 °C precursor vapor which had a higher Young's modulus had an additional peak at 1100 cm^{-1} for less relaxed network structure with lower connectivity. This result suggested that the higher Young's modulus of the 23 °C TEOS coating was only due to the higher density of the coating rather than better molecular network configuration. In other words, the TEOS coating deposited from higher temperature precursor vapor was slightly more porous and had a lower Young's modulus, albeit a better configured Si–O–Si network at the molecular scale. The BTESE coating had a broadened Si–O–Si band compared to those of TEOS coatings, with the main peak still at 1075 cm^{-1} but a minor peak at 1175 cm^{-1} because of CH$_3$ rocking absorptions in Si–O–C structures.[46] The carbon remnants reduced the density and modulus of BTESE coating compared to TEOS coatings. In the TMCTS coatings spectra, significant peaks appeared at 1050, 1100, and 1150 cm^{-1}, suggesting significant siloxane ring content from the TMCTS molecule that was directly incorporated into the coating. Some broken rings formed cage structures. The coatings with higher deposition rate had higher ring structure to network structure ratio (Figure 4c). The lower connectivity and more inner space of siloxane rings and cages resulted in the lower density and Young's modulus of TMCTS coatings (Table 2).

We observed a strong correlation between coating density and Young's modulus (Figure 5b) with higher coating density resulting in higher Young's modulus. Data for fused quartz is included.[52] A linear trend was apparent for fused quartz and the TEOS and BTESE coatings with equivalent Si–O–Si networks, as indicated by the FTIR spectra (Figure 4b). A similar linear dependence of Young's modulus on bond density has also been observed in carbon bridged hybrid glass[16] and amorphous SiC coatings,[57,58] and we conclude that the modulus can be well predicted by the mass density for the typical Si–O–Si network structured coatings in our study. Note that the TMCTS coating deposited with the higher plasma power and lower O$_2$ flow rate, which had network and locally symmetric Si–O–Si structures (Figure 4b) also followed the linear trend. However, the TMCTS coatings with lower densities and highly symmetric siloxane rings (Figure 4b) had slightly higher Young's moduli than predicted by the linear trend. That was probably because of the well preserved four-membered siloxane ring structure from the TMCTS precursor molecule. The nearly planar four-membered siloxane ring is already highly prestrained, so accommodating mechanical strain by further changing the bond angles requires higher stress. In comparison, larger rings, such as six-membered rings which are the most common in bulk amorphous silica, are puckered and can accommodate mechanical strain while maintaining the optimum Si–O–Si and O–Si–O bond angles, thus exhibiting lower modulus.[59–61] As a result, the low density TMCTS coatings in this study had higher Young's moduli than predicted by the linear trend. The dependence of Young's modulus on coating density was observed for several PECVD coatings.[62,63]

Note finally that other power law scaling between the modulus and density of hybrid silica coatings has been suggested.[59] A power law scaling of $E \approx \rho^n$ revealed a high scaling exponent for highly porous gels ($n = 3.6$) and lower values for nanoporous silicas ($n = 0.6$–1.9) prepared by surfactant-directed self-assembly.[59] The linear scaling ($n = 1$)

we observe for the higher density atmospheric plsama deposited coatings with network molecular structure is therefore consistent with the nanoporous silicas. The lower density, highly symmetric multiring structured TMCTS coatings exhibit a high scaling ($n \approx 5.9$) consistent with the other less dense forms of silica.

Adhesion Energy to Stretched PMMA Substrate. Coatings of ~600 nm thick were deposited on PMMA substrate for the evaluation of adhesion. The adhesion energy of the coatings on PMMA substrate varied from 2.1 to 16.1 J/m^2. The TEOS coatings had the lowest adhesion values, 2.6 and 2.1 J/m^2 for the 23 and 135 °C delivery temperatures T_D, respectively, although their density and Young's modulus were the highest. The adhesion energies of the TMCTS coatings were slightly higher, in the range of 3.0–5.1 J/m^2. The BTESE coatings had the highest adhesion values, 4.4, 9.8, and 16.1 J/m^2, for coatings with increasing deposition rates of 59, 95, and 159 nm/min, respectively. The highest adhesion value obtained from the BTESE coating in this study was higher than the commercial polysiloxane hard coatings on plastics.[7] XPS surface scan of the fracture surface after ADCB test confirmed that all the failures were adhesive.

To understand the different adhesion values of the TEOS and BTESE coatings, XPS depth profiles of the interfacial layer between the coating and the PMMA substrate were taken. Because of the penetration depth of the X-ray and the detector angle used, the z-resolution of the profile was ~10 nm. We assumed that the sputtering rates of the 135 °C TEOS and BTESE coating (deposition rate = 95 nm/min) were the same, because of the similar density and molecular structures of these two coatings (Table 2, Figure 4b) and the much more abundant organic species from the PMMA substrate at the interfacial region compared to the carbon remnants in the BTESE coating. Figure 7 showed the depth profiles of the interfacial layers between the TEOS or BTESE coatings and the
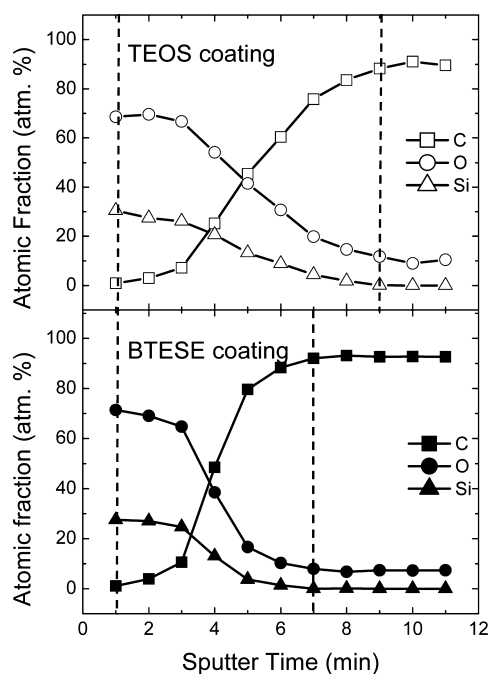

Figure 7. XPS depth profile of the interfacial layer between the PMMA substrate and the 135 °C TEOS coating and BTESE coating (deposition rate: 95 nm/min).

6595

dx.doi.org/10.1021/am301723d | ACS Appl. Mater. Interfaces 2012, 4, 6587–6598

PMMA substrate. Based on the calibrated silica sputtering rate, the TEOS interfacial layer of ~16 nm was thicker than that for the BTESE coating of ~12 nm. Note that the final C/O ratio of the PMMA substrate exceeded the stoichiometric ratio due to the decarboxylation effect of the Argon ion sputtering beam.[64] The reason for the difference in interfacial layer thickness originated from the much lower deposition rates of the TEOS coatings, from 16 to 26 nm/min, compared to 95 nm/min for the BTESE coating. The longer direct exposure of the PMMA surface to the atmospheric plasma afterglow at the initial stage of TEOS deposition therefore resulted in more substantial chain oxidation and scission and the formation of a thicker layer composed of low-molecular-weight carbon fragments on the PMMA surface. As the deposition continued, the oxidized carbon fragments mixed with the silica species and formed a weak interfacial layer, resulting in the low adhesion.

The possibility of the formation of a weak layer was confirmed by AFM characterization of a short atmospheric plasma treated PMMA surface. The surface roughness determined by AFM of pristine PMMA substrate was 0.91 ± 0.22 nm. After 5 s atmospheric plasma treatment with the same condition as for deposition, the substrate surface roughness increased to 1.2 ± 0.2 nm. However, after ethanol rinse of the treated surface, the surface roughness increased dramatically to 3.3 ± 0.5 nm. This suggested that 5 s atmospheric plasma treatment created weak, fragmented species on the PMMA surface. We estimated the TEOS coating thickness after 5 s deposition to be ~2 nm thick, and the BTESE coating to be ~8 nm thick. The PMMA was therefore exposed to the plasma for a longer period when depositing TEOS, resulting in the overoxidized substrate surface and poor adhesion.

The improved adhesion of the BTESE and TMCTS coatings compared to the TEOS coating results from their higher deposition rates which reduce the exposure of the PMMA substrate to the plasma afterglow, resulting in a functionalized but not overoxidized PMMA surface. The functionalized PMMA surface could improve the adhesion by increasing the covalent and hydrogen bonds between the coating and the substrate. In addition, the BTESE and TMCTS precursor molecules could form $R_3Si\bullet$ and $R_3SiCH_2\bullet$ radicals which then formed covalent Si−C and C−C bonds with the polymer substrate. However, the TEOS molecule has only ethoxyl functional groups and the formation of such radicals was limited. The possibility of such covalent bond formation which would significantly enhance the adhesion needs to be further investigated. Using XPS or time-of-flight secondary ion mass spectrometry to characterize the bonding species of the interface after adhesion testing may be a way to detect covalent bond formation at the interface.

The significantly enhanced adhesion of the BTESE coating deposited with Si atom density of 7.0×10^{14} atoms/cm^3 in the plasma afterglow may also be due to a molecular bridging effect.[16,65] Ethyl bridged silica sol−gel coatings were reported to dramatically improve the adhesion property compared to methylsilsesquioxane glass and pure silica.[16] The ethyl bridge in this BTESE coating as evidenced by IR could therefore result in additional covalent bonding at the interface and increase the adhesion energy.[66]

Comparing the adhesion energies of the BTESE and TMCTS coatings, the lower adhesion of the TMCTS coatings was probably because of the lower connectivity of the TMCTS coating network. Because the density and Young's modulus of the TMCTS coatings were much lower than those of the

BTESE coating, the network connectivity of the TMCTS coatings was also lower. This indicated the lower connectivity at the interface which resulted in lower adhesion values.

For the TMCTS coatings deposited in five different conditions (Table 2), the adhesion energy increased with decreasing density and Young's modulus. This may be due to the increased plasticity from molecular relaxation and rearrangements and related increasing flexibility of the Si−O−Si chains, for coatings with decreasing density and connectivity. While plasticity contributions to adhesion energy is well-known,[67] a more thorough understanding of the possible plasticity effect of these low network connectivity hybrid silica coatings awaits further study.

CONCLUSIONS

Dense silica coatings were deposited on PMMA, PC, and silicon wafers by atmospheric plasma. A high boiling temperature precursor, BTESE, as well as two widely used organosilane precursors, TEOS and TMCTS, was explored in terms of their chemical structure, delivery temperature and rate.

The deposition rate and incorporation efficiency were shown to be significantly enhanced by higher precursor delivery temperature, more reactive functional groups and preformed siloxane structure in the precursor molecule. A higher precursor molecule delivery rate also increased the deposition rate but decreased the incorporation efficiency. The composition of the coatings was also closely related to the functionality and preformed siloxane structure in the precursor molecule. The precursors with more reactive functional groups could incorporate more carbon species as well as intact preformed siloxane structure in the coating.

The Young's modulus of the coatings ranged from 6 to 34 GPa. The TEOS coatings had the highest density and Young's modulus, with the lowest deposition rate and carbon residues. The BTESE coating also had relatively high density and Young's modulus, together with slightly higher deposition rate and carbon content. The TMCTS coatings had the lowest density and Young's modulus, along with their highest deposition rate and carbon content. For the coatings with a mainly network Si−O−Si structure and higher density, there was a linear dependence of the Young's modulus on the coating density. In contrast, the less dense TMCTS coatings incorporating the highly symmetric siloxane ring structures exhibited a higher order power law scaling.

The adhesion of these coatings to the PMMA substrate was found to be affected by the deposition rate, molecular structure, coating density and Young's modulus. The TEOS coatings had the highest density and Young's modulus, but the adhesion of 2.1−2.6 J/m^2 on PMMA was low, which was due to its low deposition rate and over exposure of the PMMA substrate to the plasma afterglow. The TMCTS coatings had the highest deposition rate, the lowest density and Young's modulus, and slightly higher adhesion on PMMA in the range of 3.0−5.1 J/m^2. The slightly higher adhesion was the combinational effect of good protection of the PMMA substrate with the high deposition rate but low covalent/hydrogen bond density at the interface because of the low coating density and Young's modulus. Interestingly, the coatings deposited from BTESE had the highest adhesion in the range of 4.4−16.1 J/m^2 on the PMMA substrate. This was due to both the high deposition rate, coating density/modulus, and molecular bridging effect for the BTESE coating in the highest adhesion value.

6596

dx.doi.org/10.1021/am301723d | *ACS Appl. Mater. Interfaces* 2012, 4, 6587−6598

AUTHOR INFORMATION

Corresponding Author

*Address: IBM Almaden Research Center 650 Harry Road, K-17/E-1 San Jose, CA 95120 (G.D.); Department of Materials Science and Engineering 496 Lomita Mall, Durand Bldg., Rm. 121 Stanford University Stanford, CA 94305-4034 (R.H.D.). E-mail: gdubois@us.ibm.com (G.D.); dauskardt@stanford.edu (R.H.D.).

Notes

The authors declare no competing financial interest.

ACKNOWLEDGMENTS

ABBREVIATIONS

BTESE = 1,2-bis(triethoxysilyl)ethane
TEOS = tetraethoxysilane
TMCTS = tetramethylcyclotetrasiloxane
PMMA = poly(methyl methacrylate)
PC = polycarbonate
PECVD = plasma enhanced chemical vapor deposition
Me = methyl group
Et = ethyl group
OEt = ethoxyl group
RF = radio frequency
ATR = attenuated total reflectory
XPS = X-ray photoelectron spectroscopy
XRR = X-ray reflectivity
AFM = atomic force microscopy
ADCB = asymmetric double cantilever beam

REFERENCES

(1) Katsamberis, D.; Browall, K.; Iacovangelo, C.; Neumann, M.; Morgner, H. Prog. Org. Coat. 1997, 34, 130−134.
(2) Erlat, A. G.; Spontak, R. J.; Clarke, R. P.; Robinson, T. C.; Haaland, P. D.; Tropsha, Y.; Harvey, N. G.; Vogler, E. A. J. Phys. Chem. B 1999, 103, 6047−6055.
(3) Zhu, P. X.; Teranishi, M.; Xiang, J. H.; Masuda, Y.; Seo, W. S.; Koumoto, K. Thin Solid Films 2005, 473, 351−356.
(4) Brown, M. D.; Suteewong, T.; Kumar, R. S. S.; D'Innocenzo, V.; Petrozza, A.; Lee, M. M.; Wiesner, U.; Snaith, H. J. Nano Lett. 2010, 11, 438−445.
(5) Vasconcelos, D. C. L.; Carvalho, J. A. N.; Mantel, M.; Vasconcelos, W. L. J. Non-Cryst. Solids 2000, 273, 135−139.
(6) Lionti, K.; Toury, B.; Boissière, C.; Benayoun, S.; Miele, P. J. Sol−Gel Sci. Technol. 2012, DOI: 10.1007/s10971-012-2715-9.
(7) Kamer, A.; Larson-Smith, K.; Pingree, L. S. C.; Dauskardt, R. H. Thin Solid Films 2011, 519, 1907−1913.
(8) Hench, L. L.; West, J. K. Chem. Rev. (Washington, DC, U. S.) 1990, 90, 33−72.
(9) Zvanut, M. E.; Feigl, F. J.; Fowler, W. B.; Rudra, J. K.; Caplan, P. J.; Poindexter, E. H.; Zook, J. D. Appl. Phys. Lett. 1989, 54, 2118−2120.
(10) Xi, J. Q.; Schubert, M. F.; Kim, J. K.; Schubert, E. F.; Chen, M.; Lin, S.-Y.; Liu, W.; Smart, J. A. Nat. Photonics 2007, 1, 176−179.
(11) Schaepkens, M.; Selezneva, S.; Moeleker, P.; Iacovangelo, C. D. In High-Rate Deposition of Abrasion Resistant Coatings Using a Dual-Source Expanding Thermal Plasma Reactor; AVS: Denver, CO, U.S.A., 2003; pp 1266−1271.
(12) Theil, J. A.; Tsu, D. V.; Watkins, M. W.; Kim, S. S.; Lucovsky, G. J. Vac. Sci. Technol., A 1990, 8, 1374−1381.
(13) Nowling, G. R.; Yajima, M.; Babayan, S. E.; Moravej, M.; Yang, X.; Hoffman, W.; Hicks, R. F. Plasma Sources Sci. Technol. 2005, 14, 477−484.
(14) Pappas, D. J. Vac. Sci. Technol., A 2011, 29, 020801.
(15) Yildirim, E. D.; Besunder, R.; Pappas, D.; Allen, F.; Guceri, S.; Sun, W. Biofabrication 2010, 2, 014109.
(16) Dubois, G.; Volksen, W.; Magbitang, T.; Miller, R. D.; Gage, D. M.; Dauskardt, R. H. Adv. Mater. (Weinheim, Ger.) 2007, 19, 3989−3994.
(17) Jeong, J. Y.; Park, J.; Henins, I.; Babayan, S. E.; Tu, V. J.; Selwyn, G. S.; Ding, G.; Hicks, R. F. J. Phys. Chem. A 2000, 104, 8027−8032.
(18) Moravej, M.; Hicks, R. F. Chem. Vap. Deposition 2005, 11, 469−476.
(19) Gelest Inc. 1,2-bis(triethoxysilyl)ethane MSDS.
(20) Moravej, M.; Yang, X.; Nowling, G. R.; Chang, J. P.; Hicks, R. F.; Babayan, S. E. J. Appl. Phys. 2004, 96, 7011−7017.
(21) Alcott, G. R.; van de Sanden, R. M. C. M.; Kondic, S.; Linden, J. L. Chem. Vap. Deposition 2004, 10, 20−22.
(22) Lagendijk, A. U.S. Patent 5028566 1991.
(23) Sigma-Aldrich 2012 tetramethylcyclotetrasiloxane MSDS.
(24) Anderson, T. L. Fracture Mechanics: Fundamentals and Applications; CRC Press: Boca Raton, FL, 2005.
(25) Suo, Z. G.; Hutchinson, J. W. Mater. Sci. Eng., A 1989, 107, 135−143.
(26) Kanninen, M. F. Int. J. Fract. 1973, 9, 83−92.
(27) Deshmukh, S. C.; Aydil, E. S. J. Vac. Sci. Technol., A 1995, 13, 2355−2367.
(28) Bartram, M. E.; Moffat, H. K. J. Vac. Sci. Technol., A 1994, 12, 1027−1031.
(29) Roger, C.; Corbitt, T. S.; Hampdensmith, M. J.; Kodas, T. T. Appl. Phys. Lett. 1994, 65, 1021−1023.
(30) Liao, N. M.; Li, W.; Jiang, Y. D.; Kuang, Y. J.; Qi, K. C.; Wu, Z. M.; Li, S. B. Appl. Phys. A: Mater. Sci. Process 2008, 91, 349−352.
(31) Martins, R.; Silva, V.; Ferreira, I.; Domingues, A.; Fortunato, E. Mater. Sci. Eng., B 2000, 69, 272−277.
(32) Liao, N. M.; Li, W.; Jiang, Y. D.; Wu, Z. M.; Qi, K. C.; Li, S. B. Philos. Mag. 2008, 88, 3051−3057.
(33) Walsh, R. Acc. Chem. Res. 1981, 14, 246−252.
(34) Walsh, R. The Chemistry of Organic Silicon Compounds; Patai, S., Rappoport, Z., Eds.; John Wiley and Sons, Ltd: Chichester, U.K., 1989; pp 371−391.
(35) Blanksby, S. J.; Ellison, G. B. Acc. Chem. Res. 2003, 36, 255−263.
(36) Babayan, S. E.; Jeong, J. Y.; Schutze, A.; Tu, V. J.; Moravej, M.; Selwyn, G. S.; Hicks, R. F. Plasma Sources Sci. Technol. 2001, 10, 573−578.
(37) Fuchs, G.; Melinon, P.; Aires, F. S.; Treilleux, M.; Cabaud, B.; Hoareau, A. Phys. Rev. B: Condens. Matter Mater. Phys. 1991, 44, 3926−3933.
(38) Hoogeveen, N. G.; Stuart, M. A. C.; Fleer, G. J. J. Colloid Interface Sci. 1996, 182, 133−145.
(39) Rau, C.; Kulisch, W. Thin Solid Films 1994, 249, 28−37.
(40) Schafer, J.; Foest, R.; Quade, A.; Ohl, A.; Weltmann, K. D. J. Phys. D: Appl. Phys. 2008, 41.
(41) Huang, C.; Liu, C.-H.; Wu, S.-Y. Surf. Interface Anal. 2009, 41, 44−48.
(42) Delplancke, M. P.; Powers, J. M.; Vandentop, G. J.; Salmeron, M.; Somorjai, G. A. J. Vac. Sci. Technol., A 1991, 9, 450−455.
(43) Matsuda, Y.; King, S. W.; Bielefeld, J.; Xu, J.; Dauskardt, R. H. Acta Mater. 2012, 60, 682−691.
(44) Grill, A.; Neumayer, D. A. J. Appl. Phys. 2003, 94, 6697−6707.
(45) Qi, H.; Han, J.; Xu, N. J. Membr. Sci. 2011, 382, 231−237.
(46) Matos, M. C.; Ilharco, L. M.; Almeida, R. M. J. Non-Cryst. Solids 1992, 147, 232−237.
(47) Pandey, K. K. J. Appl. Polym. Sci. 1999, 71, 1969−1975.

6597

dx.doi.org/10.1021/am301723d | ACS Appl. Mater. Interfaces 2012, 4, 6587−6598

(48) Gates, S. M.; Dubois, G.; Ryan, E. T.; Grill, A.; Liu, M.; Gidley, D. *J. Electrochem. Soc.* **2009**, *156*, G156−G162.

(49) Elimelech, M. *J. Colloid Interface Sci.* **1994**, *164*, 190−199.

(50) Zou, J. W.; Reichelt, K.; Schmidt, K.; Dischler, B. *J. Appl. Phys.* **1989**, *65*, 3914−3918.

(51) Ishida, M.; Fujita, J.; Ichihashi, T.; Ochiai, Y.; Kaito, T.; Matsui, S. *J. Vac. Sci. Technol., B* **2003**, *21*, 2728−2731.

(52) Oliver, W. C.; Pharr, G. M. *J. Mater. Res.* **1992**, *7*, 1564−1583.

(53) Oliver, M. S.; Dubois, G.; Sherwood, M.; Gage, D. M.; Dauskardt, R. H. *Adv. Funct. Mater.* **2010**, *20*, 2884−2892.

(54) Lin, Y. B.; Tsui, T. Y.; Vlassak, J. J. *J. Electrochem. Soc.* **2006**, *153*, F144−F152.

(55) Park, E. S.; Ro, H. W.; Nguyen, C. V.; Jaffe, R. L.; Yoon, D. Y. *Chem. Mater.* **2008**, *20*, 1548−1554.

(56) Volksen, W.; Miller, R. D.; Dubois, G. *Chem. Rev. (Washington, DC, U. S.)* **2010**, *110*, 56−110.

(57) Khakani, M. A. E.; Chaker, M.; Jean, A.; Boily, S.; Kieffer, J. C. *J. Mater. Res.* **1994**, *9*, 96−103.

(58) Khakani, M. A. E.; Chaker, M.; Hern, M. E. O.; Oliver, W. C. *J. Appl. Phys.* **1997**, *82*, 4310−4318.

(59) Fan, H.; Hartshorn, C.; Buchheit, T.; Tallant, D.; Assink, R.; Simpson, R.; Kissel, D. J.; Lacks, D. J.; Torquato, S.; Brinker, C. J. *Nat. Mater.* **2007**, *6*, 418−423.

(60) Keeffe, M. O.; Gibbs, G. V. *J. Appl. Phys.* **1984**, *81*, 876−879.

(61) Galeener, F. L. in *The Structure of Non-Crystalline Materials*; Gaskell, P. H., Parker, J. M., Davis, E. K., Eds; Taylor and Francis: London, 1982; pp 337−359.

(62) Taylor, J. A. *J. Vac. Sci. Technol., A* **1991**, *9*, 2464−2468.

(63) Huang, H.; Winchester, K. J.; Suvorova, A.; Lawn, B. R.; Liu, Y.; Hu, X. Z.; Dell, J. M.; Faraone, L. *Mater. Sci. Eng., A* **2006**, *435−436*, 453−459.

(64) Mahoney, C. M. *Mass Spectrom. Rev.* **2009**, 247−293.

(65) Maidenberg, D. A.; Volksen, W.; Miller, R. D.; Dauskardt, R. H. *Nat. Mater.* **2004**, *3*, 464−469.

(66) Launey, M. E.; Ritchie, R. O. *Adv. Mater. (Weinheim, Ger.)* **2009**, *21*, 2103−2110.

(67) Lane, M.; Dauskardt, R. H.; Vainchtein, A.; Gao, H. J. *J. Mater. Res.* **2000**, *15*, 2758−2769.

6598

dx.doi.org/10.1021/am301723d | *ACS Appl. Mater. Interfaces* 2012, 4, 6587−6598